Low and optically thin cloud measurements using a Raman–Mie lidar

Yonghua Wu,* Shuki Chaw, Barry Gross, Fred Moshary, and Sam Ahmed

Optical Remote Sensing Laboratory, The City College of New York, New York, New York 10031, USA

*Corresponding author: yhwu@ccny.cuny.edu

Received 4 September 2008; revised 5 December 2008; accepted 27 January 2009;
posted 29 January 2009 (Doc. ID 100867); published 19 February 2009

We analyze the potential of measuring low-altitude optically thin clouds with a Raman-elastic lidar in the daytime. Optical depths of low clouds are derived by two separate methods from nitrogen Raman and elastic-scattering returns. By correcting for aerosol influences with the combined Raman–elastic returns, Mie retrievals of low-cloud optical depth can be dramatically improved and show good agreement with the direct Raman retrievals. Furthermore, a lidar ratio profile is mapped out and shown to be consistent with realistic water phase cloud models. The variability of lidar ratios allows us to explore the distribution of small droplets near the cloud perimeter. © 2009 Optical Society of America

OCIS codes: 010.3640, 280.3640, 280.0280.

1. Introduction

Low-altitude clouds play an important role in global climate forcing, weather, and precipitation [1,2]. In particular, low clouds often have large liquid water path (LWP) and are involved in interactions with anthropogenic aerosols and the atmospheric boundary layer [3–5]. Unfortunately, for satellite sensors with visible and near-infrared channels, measurement of low and optically thin clouds from space is very difficult due to their partial transparency, land surface emission, and the fact that they are relatively warm [6]. Even though a single layer of low cloud usually simplifies modeling, intercomparisons among different retrievals and instruments indicate large discrepancies of LWP and optical depth [3]. Therefore, it is a significant challenge to accurately measure and model their optical and microphysical properties in order to assimilate them into global climate models [2,3,6]. On the other hand, lidar has been extensively demonstrated for observing cloud properties. However, most previous work [7–10] with lidar techniques concentrates on high and thin cirrus clouds at night. To measure thin cloud optical depth, Young [7] presented a method based solely on the elastic lidar returns above and below the cloud layer. In that method, the actual lidar elastic returns below and above clouds are fitted to theoretical molecular scattering returns, which work well for high cirrus because any residual aerosols can be ignored at high altitudes both above and below the cloud. Cadet *et al.* [10] showed that the variability of the lidar ratio (extinction-to-backscatter ratio) within the clouds significantly influences cloud optical depth retrieval in the particular integration method using the elastic returns. Ansmann *et al.* [9] compared Raman-elastic-scattering inversions and found that the Klett solution [11] of the cirrus extinction profile and optical depth strongly depended on the lidar ratio variation along the measuring range.

For low-altitude clouds, a direct measurement of the extinction and, therefore, of cloud optical depth (COD) using a nitrogen (N_2) Raman lidar is possible. Unfortunately, the weak Raman signal makes it difficult to apply to clouds with significant optical depth (particularly in daytime conditions). Furthermore, the low signal-to-noise ratio (SNR) inherent in pulling out the extinction coefficient within the cloud makes it difficult to rely solely on the Raman retrieval of extinction.

0003-6935/09/061218-10$15.00/0

To address this issue, it would be advantageous to use multiple approaches to verify COD measurements. A reasonable approach is to apply the regression approach commonly used for high cirrus. However, for low clouds, corrections for aerosol influences have to be carefully treated due to high aerosol loading in the lower atmosphere. For this correction, the accurate backscatter profiles from Raman–Mie lidar during clear sky or cloud breaks conditions would be helpful because they are not sensitive to lidar-ratio.

We focus on using multiple retrieval methods to explore the accuracy and limits of measuring low-altitude optically thin cloud measurements with a Raman–Mie lidar under daylight conditions and to assess the errors due to heavy aerosol loading above and below the cloud. To begin, cloud base and cloud top altitudes are identified through a wavelet transform analysis of elastic returns. After defining the cloud boundary levels, optical depths of low-altitude clouds are derived using two independent methods. The first method is based on a direct measurement of the extinction coefficient profile in the cloud using the direct N_2 Raman-return retrieval method [9] followed by an integration of the extinction profile of the cloud between the cloud boundaries. This method will be referred to as "Raman retrieval." The second method is based on the regression matching technique [7] where the COD results in a modification of the regression slopes obtained both above and below the cloud. This method will be referred to as "Mie retrieval." When comparing Mie retrieval to Raman retrieval, significant errors result if the aerosol loading above and below the cloud is not quantified. One simple correction for the Mie-retrieval method is to use the Fernald inversion [12] method with an *a priori* lidar ratio in the clear sky patches. However, we show that an accurate correction for aerosol influences can only be achieved by retrieving the aerosol profiles using the combined N_2 Raman and elastic returns. When this correction is used, we find that consistent results are obtained between the Raman-retrieval method and the corrected Mie-retrieval method as long as optical depths are smaller than 1.5 at 355 nm. Once the extinction profiles are validated, we can then calculate the lidar ratio within these clouds. In fact, integrated lidar ratio measurements obtained in this manner are shown to be consistent with those expected from water phase clouds calculated from Mie scattering using reasonable gamma distributed water droplet size distribution models. From this model, we also find significant variation of the lidar ratios that allows us to probe for small droplets within the bulk cloud.

In Section 2, the Raman–Mie lidar system is briefly described. In Section 3, the retrieval algorithms used for processing the lidar data are developed and, in Section 4, results of the intercomparisons are provided illustrating the need for a combined Raman–Mie processing approach. Furthermore, the lidar-ratio profiles are obtained and shown to be consistent with water phase clouds and the variability of the lidar ratio is explored. Finally, in Section 5, multiple-scattering effects that directly impact COD measurements are quantified using a simple multiple-scattering model for our lidar specifications and cloud properties geometries.

2. Instrument Description of Raman-Mie Lidar

A multiple-wavelength Raman–Mie lidar located on the City College of New York campus (40.82°N/73.95°W) in New York City is in operation, providing aerosol, water vapor, and cloud measurements. The Nd:YAG laser emits at 355–532–1064 nm with a 30 Hz repetition rate and a 7 ns pulse length. The configuration of the optical receiver is given in Fig. 1. A Newtonian telescope with diameter 50.8 cm is used to collect all the backscatter returns. Elastic scattering (Mie + Rayleigh) returns at the three wavelengths, together with N_2 and H_2O Raman-shifted returns excited by a 355 nm laser beam are simultaneously detected. Photomultiplier tubes (PMT) are employed to detect UV–visible returns while a Si avalanche photodiode (APD) detector is used for the 1064 nm channel. Narrow-band interference filters (Barr Associates) are used to suppress the skylight background noise. The interference filters for the Raman channels have a specifically high blocking ratio at the 355 nm laser line, which can efficiently reduce the cross talk of elastic return at that channel. This capability is well verified by comparing strong elastic returns to weak Raman returns by low clouds. A multichannel Licel transient recorder acquires the lidar signal data with the combined analog-to-digital converter (40 MHz, 12 bit) and photon-counting (250 MHz) techniques. The lidar return profiles are recorded at 1 min time averaging with a nominal 3.75 nm range resolution. With coaxial transmitter–receiver geometry, full return signals starting from an altitude of 300 m can be detected, making this lidar efficient for detecting low clouds. Currently, regular observations are performed in the daytime for three days per week on average. The main specifications are listed in Table 1.

3. Retrieval of Cloud Optical Depth with a Mie–Raman lidar

Here we provide a brief overview of extinction and backscatter retrievals with the combined Raman–Mie lidar. Considering only single-scattering returns, the extinction coefficient of particulates (aerosol or cloud) can be directly derived from the N_2 Raman return [13,14]:

$$\alpha_p(\lambda_0,z)=\frac{1}{1+\left(\frac{\lambda_N}{\lambda_0}\right)^{-v}}\left\{\frac{\mathrm{d}}{\mathrm{d}z}\left[\ln\frac{N(z)}{P(\lambda_N,z)z^2}\right]-\alpha_m(\lambda_0,z)\left[1+\left(\frac{\lambda_N}{\lambda_0}\right)^{-4}\right]\right\}, \quad (1)$$

where α is the extinction coefficient and subscripts p and m refer to particles and molecules, respectively, and $P(\lambda_N,z)$ is the N_2 Raman-return intensity at

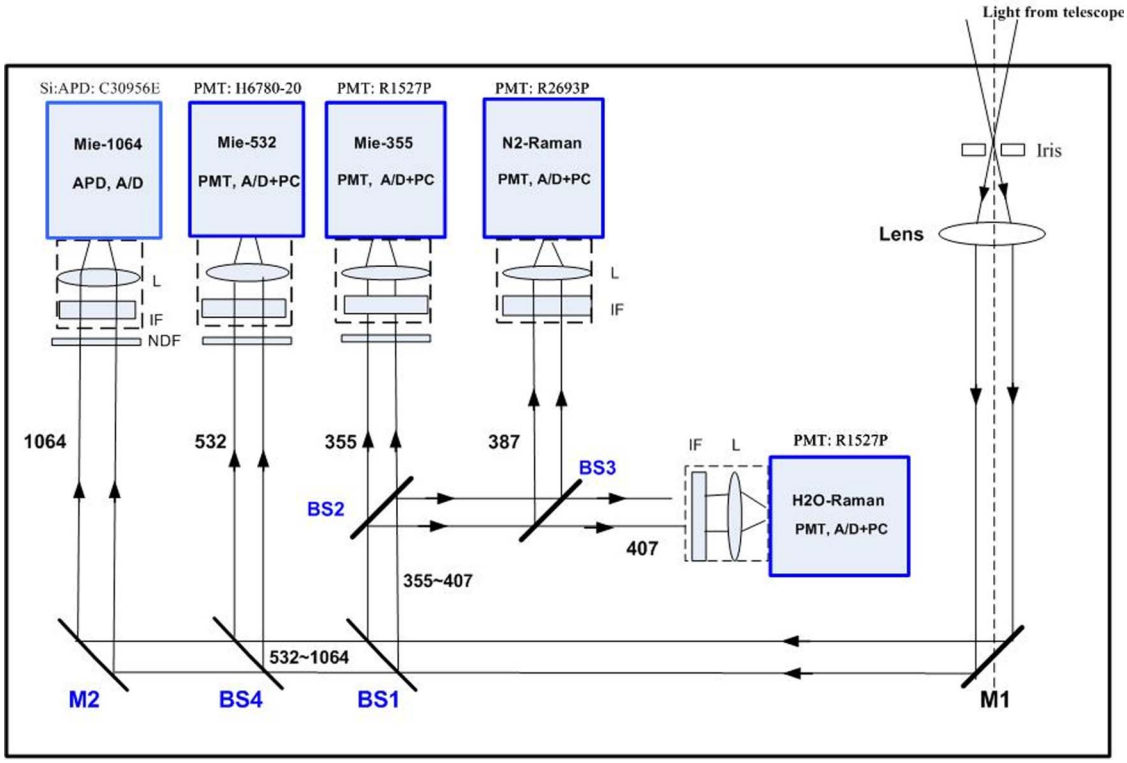

Fig. 1. (Color online) Optical layout of the Raman–Mie lidar receiver.

range z. $N(z)$ is the molecular number density. Here, λ is the wavelength where subscripts o and N refer to the laser and N_2 Raman-shifted wavelengths, respectively. The Angstrom coefficient ν is taken to be 1.2 for aerosol and 0 for cloud [9,14]. α_p is changed to α_c in Eq. (1) for the cloud. Integrating the Raman-retrieved extinction profile from cloud base z_b to top z_t, provides the first direct approach (i.e., Raman method as described in Section 1) for the determination of the COD:

$$\tau_C = \int_{z_b}^{z_t} \alpha_c(z)\mathrm{d}z. \tag{2}$$

This method directly solves the cloud extinction coefficient without assuming a lidar ratio and a calibrating system constant, but its measuring capability would be limited by the much weaker Raman returns than elastic returns.

From the N_2 Raman and elastic-scattering returns, particle-scattering ratio $R(\lambda_0,z)$ and backscatter $\beta(\lambda_0,z)$ can be written as

$$\begin{aligned} R(\lambda_0,z) &= \frac{\beta_p(\lambda_0,z)+\beta_m(\lambda_0,z)}{\beta_m(\lambda_0,z)} \\ &= \frac{P(\lambda_0,z)}{P(\lambda_N,z)} R(\lambda_o,z_{\mathrm{ref}}) \frac{P(\lambda_{N2},z_{\mathrm{ref}})}{P(\lambda_0,z_{\mathrm{ref}})} \\ &\quad \times \frac{\exp\left\{-\int_z^{z\mathrm{ref}}[\alpha_p(\lambda_0,z')+\alpha_m(\lambda_0,z')]\mathrm{d}z'\right\}}{\exp\left\{-\int_z^{z\mathrm{ref}}[\alpha_p(\lambda_N,z')+\alpha_m(\lambda_N,z')]\mathrm{d}z'\right\}}, \end{aligned} \tag{3}$$

$$\beta_p(\lambda_0,z) = [R(\lambda_0,z)-1]\beta_m(\lambda_0,z) \tag{4}$$

where $\beta_p(\lambda_0,z)$ and $\beta_m(\lambda_0,z)$ refer to particle and molecular backscatter coefficients, respectively, at the laser wavelength and range z. Here, z_{ref} is a reference altitude where the aerosol-scattering ratio R_{ref} is assumed to be known and is usually chosen to be within an aerosol-free region. Molecular extinction and number density are calculated from radiosonde data at the Brookhaven National Laboratory site (Upton, New York, National Weather Service), which

Table 1. Main Specifications of Raman–Mie Lidar System at City College of New York

Laser	Quanta-Ray PRO-230 Nd:YAG, 30 Hz 950 mJ at 1064 nm, 475 mJ at 532 nm, 300 mJ at 355 nm
Telescope	Newtonian, $f/3.5$; diameter: 50.8 cm; FOV, 1.5 mrad
Interference Filters	Barr Associates Inc., central wavelength/bandwidth/peak transmission Mie channel, 1064, 532, $355/0.3\sim1$ nm/$T>50\%$; N_2 Raman, 386.7/0.3 nm/$T=65\%$; H_2O (vapor) Raman, 407.5/0.5 nm/$T=65\%$
Detectors	EG&G Si:APD for 1064 nm; Hamamatsu PMT: H6780-20, R2693P, R1527P
Data acquisition	Licel TR 40-160, 12 bit and 40 MHz A/D, 250 MHz photon-counting
Range resolution	3.75 m

is about 90 km from the lidar site. The ratio of the transmission terms in Eq. (3) is usually close to unity because of the small difference between wavelengths λ_0 and λ_N. Finally, the extinction-to-backscatter ratio, or lidar ratio, or the S ratio can be calculated. The lidar ratio depends on the physical and chemical properties of particles.

The second method for deriving COD following Young's approach [7] first requires the calculation of the molecular-scattering return according to

$$P_m(\lambda_0, z) = \beta_m(\lambda_0, z) \times T_m^2(\lambda_0, z)/z^2. \tag{5}$$

Once the molecular profile is calculated, the measured elastic-scattering returns are regressed against the molecular profile both below and above the cloud. Taking into account that aerosol layers can exist both above and below the cloud, the regressed slopes below the cloud (z_1 to z_2) and above the cloud (z_3 to z_4) can be written as

$$\begin{aligned} m_{\text{bot}} &= CT_a^2(z_0, z_1)\bar{R}_{\text{bot}}(z_1, z_2), \\ m_{\text{top}} &= CT_a^2(z_0, z_1)\bar{R}_{\text{top}}(z_3, z_4)T_c^2, \end{aligned} \tag{6}$$

where C is the lidar system constant, z_0 is the initial lidar altitude, T_a and T_c are aerosol and cloud transmissions, respectively, and $\bar{R}$ is the average of the aerosol-scattering ratio over the regression ranges. In the regressions performed above, we assume a constant aerosol-scattering ratio and ignore aerosol attenuation within the regressed range window. This window is variable dependent on cloud height, aerosol variability, and SNR, but it has been found that regression windows between 0.1 and 0.2 km, where aerosol-scattering ratios generally vary little, are suitable. Clearly, COD can be derived from Eq. (6) as

$$\tau_C = \left[\log\left(\frac{m_{\text{bot}}}{m_{\text{top}}}\right) - \log\left(\frac{\bar{R}_{bot}}{\bar{R}_{top}}\right)\right]/2, \tag{7}$$

where $\log(\bar{R}_{\text{bot}}/\bar{R}_{\text{top}})$ is called the aerosol correction factor and the COD uncertainty is given as

$$\delta\tau_C = \frac{1}{2}\sqrt{\left(\frac{\delta m_{\text{bot}}}{m_{\text{bot}}}\right)^2 + \left(\frac{\delta m_{\text{top}}}{m_{\text{top}}}\right)^2 + \left(\frac{\delta\bar{R}_{\text{bot}}}{\bar{R}_{\text{bot}}}\right)^2 + \left(\frac{\delta\bar{R}_{\text{top}}}{\bar{R}_{\text{top}}}\right)^2}, \tag{8}$$

This second method to obtain optical depth from Eq. (7) using elastic-returns regression is what we referred to in Section 1 as Mie retrieval. This method is especially accurate for high and thin cirrus because nearly free-aerosol layers exist below and above the cloud so that aerosol influence can be ignored. On the other hand, aerosol loading is usually high at low altitudes, so it is necessary to estimate the aerosol item $R_{\text{bot}}/R_{\text{top}}$ in Eq. (7). Clearly, the ratio $(R_{\text{bot}}/R_{\text{top}})$ can be obtained from the combined Raman–Mie signals, as seen in Eq. (3) and, moreover, it is quite insensitive to the assigned $R_{z\text{ref}}$ and lidar ratio. Because of poor signal penetration of the Raman channel, we prefer to perform this analysis in clear sky patches found within the cloud decks and assume that the vertical structure of the aerosol-scattering ratio is fairly stable over small time periods. This is quite reasonable for the low optical thickness cases considered where clear sky patches are numerous. This is the unique advantage of Raman–Mie lidars over elastic lidar retrievals alone, where the aerosol ratios would depend strongly on the assumed lidar ratio and the reference value R_{ref} (which is not the case when the Mie–Raman lidar is used). The level of improvement in deriving COD due to more robust aerosol correction is explored in Subsection 4.B. In all subsequent discussion, retrievals using only the N_2 Raman signals in Eq. (2) are referred to Raman retrieval, while the use of elastic returns with regression in Eq. (7) is referred to Mie retrieval for deriving the COD.

In both retrieval methods an important issue is to accurately and objectively determine the cloud base and top. For this purpose, a wavelet transform analysis of elastic returns is used. The covariance transform is defined as [15,16]

$$W(a, b) = \int_{z_0}^{z'} \left[P(z)h\left(\frac{z-b}{a}\right)\right] \mathrm{d}z, \tag{9}$$

where $P(z)$ is the elastic-scattering lidar signal from range z, h is the wavelet function, and a and b are the dilation and translation parameters of the wavelet (Mexican hat) function, respectively. The locations of cloud base and top can be found by minimizing the covariance transform over a wide distribution of wavelet parameters. This method works well for the single-layer cases we are considering.

4. Result and Discussion

A. Cloud Profiles

To illustrate the capability of the Raman lidar to provide cloud properties in daylight, Figs. 2(a) and 2(b) show a representative profile of cloud optical parameters obtained on 15 March 2006. A cloud layer clearly appears in the backscatter profile at between 2 and 3 km altitude. Raman processing allows us to calculate the profile of cloud extinction-to-backscatter ratios, or lidar ratios, which we observe are significantly smaller than those of aerosols. In particular, we find the mean value of cloud lidar ratios at 355 nm is 18.6 sr with a standard deviation of 3.9 sr. This value is comparable with previous observations and numerical analysis [17,18] and is consistent with Mie-scattering calculations using a normalized gamma mode of cloud droplet size distribution. In particular, the value of the lidar ratio based on the Mie-scattering model is calculated to be 18.9 ± 0.4 sr at 355 nm over the wide range of mode parameters [17].

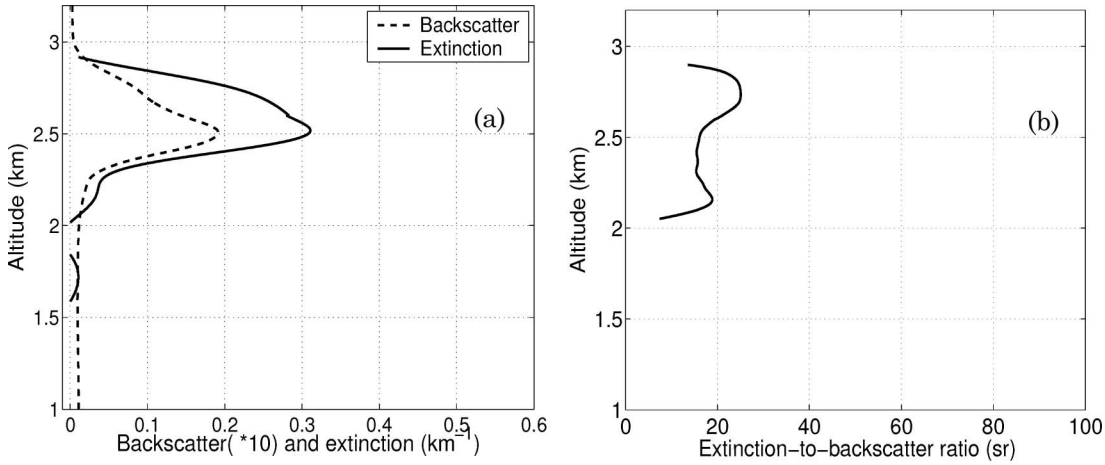

Fig. 2. (a) Cloud backscatter, extinction coefficient, and (b) their ratio at 355 nm on 15 March 2006.

B. Regression of Cloud Optical Depth with Elastic Returns

Figure 3(a) shows the background noise subtracted elastic and N_2 Raman-scattering returns on 6 April 2006. A 10 min data average is used to reduce the noise. Elastic returns indicate a cloud layer over 1.5–1.9 km altitude, while the N_2 Raman signal shows a large gradient caused by cloud attenuation in this range. In the figure, the range intervals used in the regression are also marked both below and above the cloud for subsequent Mie retrieval of COD. Figure 3(b) plots the covariance of the wavelet transform of elastic returns. Clearly, cloud base and top are well identified by the minimal values of covariance.

Figure 4 shows the regressions details for the cloud optical depth on 16 June 2006 for different times. Eight vertical profiles are plotted in Fig. 4(a), which display cloud in the range of 2.3–3.3 km. In these cases, high aerosol loading appears below the cloud with overall mean aerosol-scattering ratios ranging from 2.13–2.76 below the cloud. On the other hand, aerosol loading above the cloud is found to vary with the scattering ratio in the 1.056–1.063 range. Figure 4(b) plots CODs derived independently using both the Raman-retrieval and elastic-retrieval methods. We see clearly that, without correcting for the aerosol -scattering ratio, a systematic and significant overestimate of optical depth using the Mie-retrieval method (circles) is made. After suitably correcting for the aerosols, the Mie retrieval (squares) shows good agreement with that of Raman retrieval.

Another aspect of COD retrieval to consider is the fact that, without the Raman returns, particularly below the cloud, the correction factor for the aerosol ratio is expected to be significantly less accurate. To see this clearly, we have reanalyzed the optical depth retrieval using the Mie-scattering method but using the correction factors obtained only from the elastic channel in which an assumption on the lidar S ratio is needed. The results of this retrieval relative to the combined Raman–Mie approach to correct for the aerosol ratio are given in Fig. 5. In this figure, [Mie-uncor] refers to Mie retrieval without aerosol

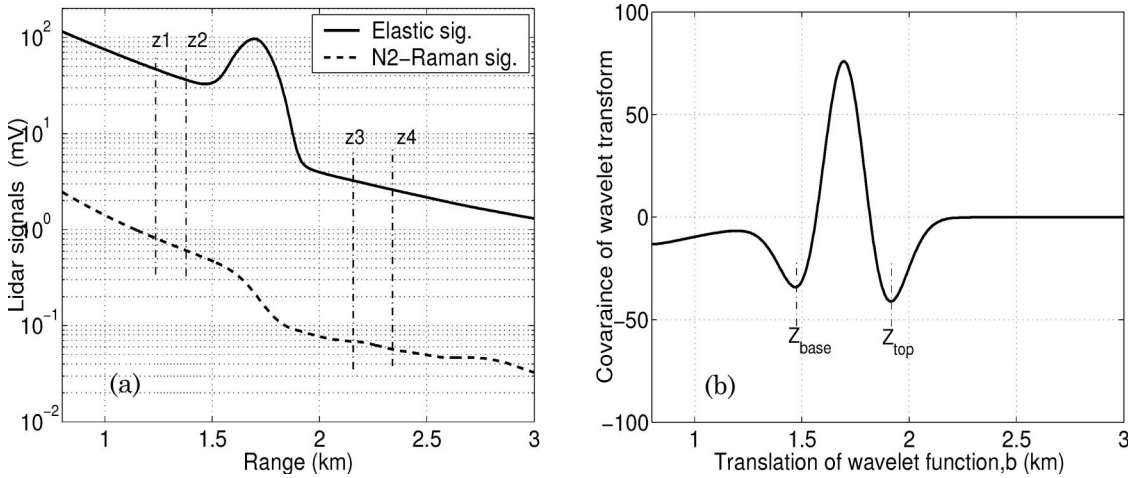

Fig. 3. (a) Elastic- and N_2 Raman-scattering signals and (b) covariance of wavelet transform on 6 April 2006.

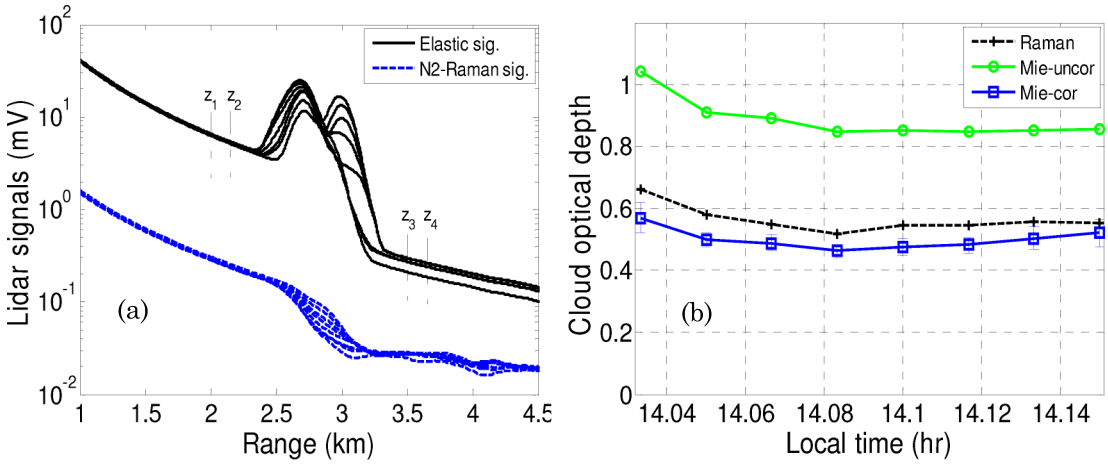

Fig. 4. (Color online) (a) Elastic- and N_2 Raman-scattering signals and (b) comparison of cloud optical depth retrieval on 16 June 2006. Raman, Raman retrieval; Mie-uncorr., Mie retrieval without aerosol correction; Mie-cor, Mie retrieval with aerosol correction.

correction, [Mie-Cor-1] refers to the case where only the elastic channel was used to retrieve the aerosol correction factor, while [Mie-Cor-2] refers to the case where the combined Raman–Mie signals are used for the aerosol correction. Clearly, a significant improvement is obtained when both the Raman and Mie lidar channels are used together.

Another concern is the fact that high COD will significantly attenuate the lidar signal, degrading the retrieval, particularly when the N_2 Raman profiles are used. In addition, the strong background signal noise in the daytime will significantly reduce the SNR. These results are seen in Fig. 6(a), which shows that, for sufficiently high COD, the N_2 Raman signal degrades below the noise threshold prior to the cloud threshold, unlike the elastic return. This results in a clear underestimation of COD using the Raman-return technique for high COD, as illustrated in Fig. 6(b). In this situation, the previous aerosol-scattering ratio profile derived from Raman-elastic returns will be used for the aerosol correction in Mie retrieval. It should, however, be pointed out that, if the degraded signal is still used to calculate extinction coefficient, the error may not always be biased low but can lead to noise-induced overestimates of extinction.

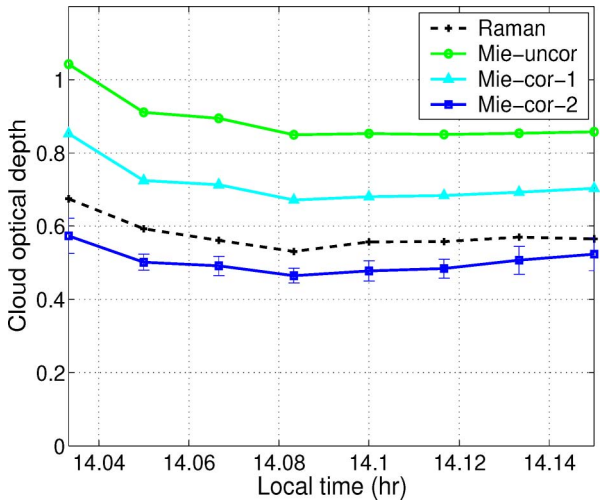

Fig. 5. (Color online) Comparison of cloud optical depth retrievals. Mie-uncor, Mie retrieval without aerosol correction; Mie-cor-1, Mie retrieval with aerosol correction from only the elastic returns; Mie-cor-2, Mie retrieval with aerosol correction from the combined Raman-elastic return.

C. Comparisons of Cloud Optical Depth Between Raman and Mie Retrievals

A representative example (15 March 2006) for a large time interval in which the COD undergoes significant change is shown in Figs. 7(a)–7(d). Range-square corrected elastic returns are plotted in Fig. 7(a), which characterize cloud heights of 1.8–3 km marked by the two lines. Complementary radiosonde data are used to identify that the cloud is most likely water phase dominated. As Fig. 7(b) shows, after aerosol contamination is eliminated, the two retrievals are nearly coincident with each other and CODs vary from 0.1 to 1.7 at a 355 nm wavelength. A good correlation between the retrievals is seen in Fig. 7(c) , with $R^2 = 0.959$. However, we do note that discrepancies become larger at higher CODs, as expected. The mean and standard deviation of lidar ratios in cloud layers are shown in Fig. 7(d) and it is observed that they mostly fluctuate about the 20 sr line with standard deviation of 6.3 sr, indicative of the dominance of the water phase in the cloud.

To assess these methods over a larger data sample, a 17 d data set with a total of 2042 pair points is statistically analyzed. The results are shown in Fig. 8. Figure 8(a) illustrates a strong correlation of $R^2 = 0.94$ with a regression slope close to 1.0. Clearly, data pairs begin to scatter at larger CODs. In Fig. 8(b), the mean values of the absolute differences are calculated as a function of COD. Over a wide range of COD (i.e., 0.3 to 1.5), fractional errors are of the order of 10% but the error gets larger as COD goes higher than 1.5.

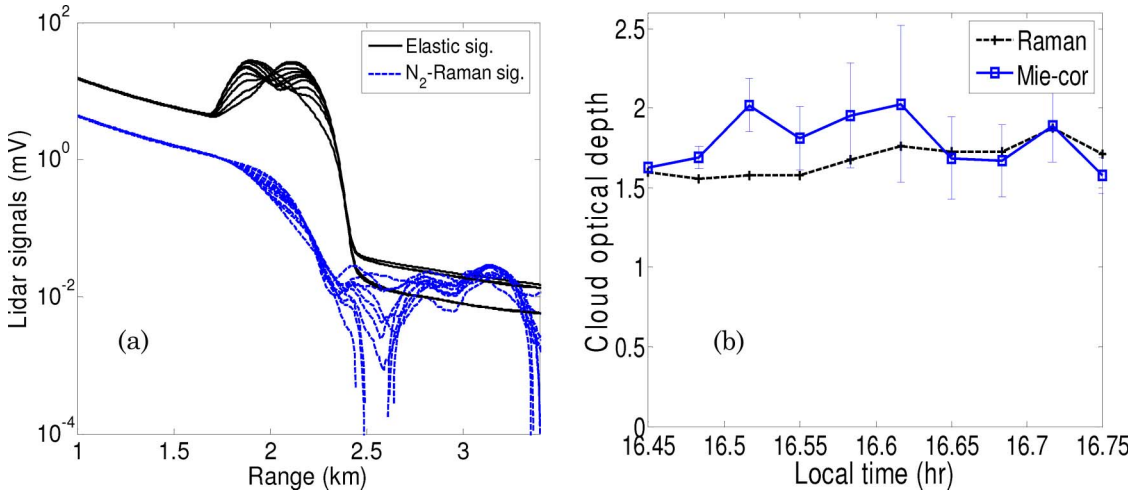

Fig. 6. (Color online) (a) N_2 Raman- and elastic-scattering signal penetration potential for relatively high COD illustrating the degradation of the Raman signal within the cloud and (b) the resultant COD comparison.

D. Varied Lidar Ratios of Low Clouds: Implication for Droplet Size

A strong agreement of the COD retrieval provides an independent validation on the accuracy of both the extinction and backscatter vertical profile within the cloud, which allows us to estimate the cloud parameters of interest. Figure 9 plots a group of cloud optical parameters, including backscatter, extinction, and lidar ratio over the cloud cross section. In this case, Raman-retrieved CODs vary over 0.1–0.3; both N_2 Raman- and elastic-scattering returns can penetrate the cloud layer well so that the lidar ratio can be derived. If the cloud was dominated by ice crystals, a single channel lidar ratio would not be able to estimate the size properties. However, if the cloud is in the water phase, a water-drop model based on a normalized gamma size distribution of spherical particles [17,19] can be developed, which allows us to

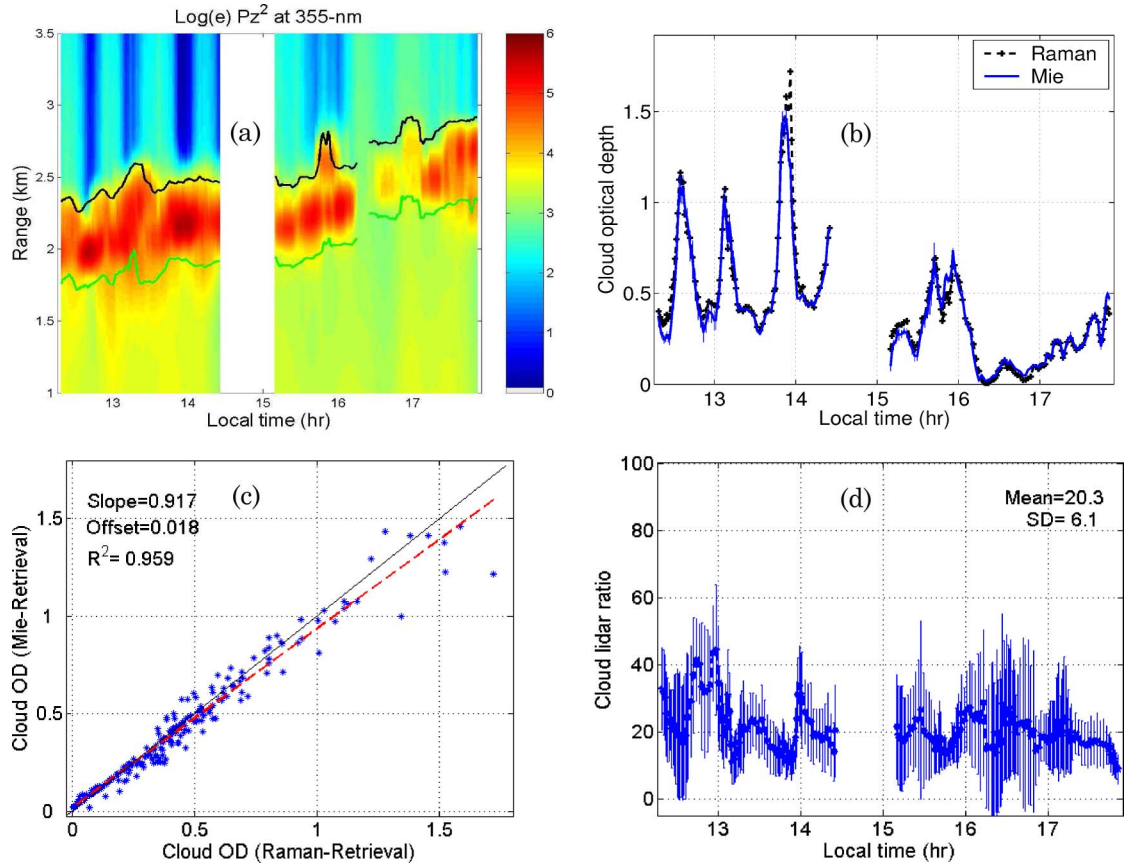

Fig. 7. (Color online) (a) Log range-square corrected elastic returns, (b) Raman- and Mie-retrieved cloud optical depths, (c) the correlation, and (d) the average and standard deviation of lidar ratios in clouds on 15 March 2006.

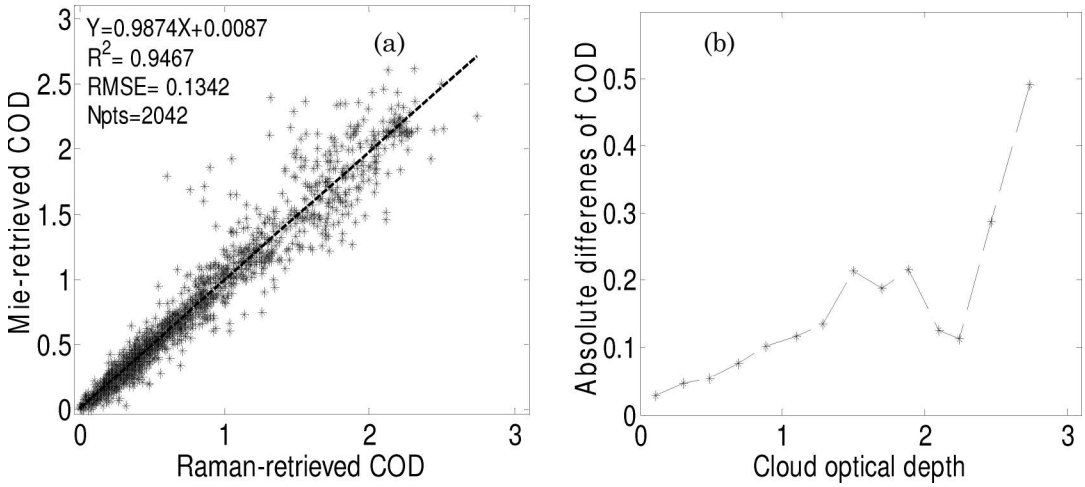

Fig. 8. (a) Correlation and (b) absolute differences among Raman- and Mie-retrieved cloud optical depths.

roughly connect the lidar ratio to an effective droplet mean diameter. The model calculated lidar ratios versus water droplet effective diameters are shown in Fig. 9(b), with the mode width parameter μ given the value of 2. Clearly, lidar ratios show a strong dependence on the effective diameters for small cloud droplets ($<3\,\mu$m) and then become fairly stable for droplet sizes of 3–20 μm, with a value of 20 sr. This is in agreement with lidar ratios obtained in dense portions of the cloud, which confirms the basic assumption that the cloud is primarily in water phase. Also, we see that, as we extend to the cloud boundaries, the lidar ratio increases markedly and this implies the presence of smaller droplets, such as would be associated either with new condensation or evaporation of the droplets near the cloud edge. Additional improvements in the range of droplet size retrieval can be obtained if we include long wavelength backscatter, as well as being able to more accurately distinguish ice from water phase. In particular, Eberhard [19] has discussed a similar approach to determining droplet size according to lidar ratio at a long laser wavelength ($\sim$10.6 μm). Further analysis is needed to explore this interesting phenomenon, which would be of great interest for the microphysical and dynamic processes of low clouds.

In evaluating the lidar ratio, we needed to ensure that all measurements were taken in the cloud interior. To verify that these measurements are from the cloud, histograms of particles' backscatter coefficients are plotted in Fig. 9(c). The dotted curve shows the data from 1.9 to 3.1 km altitudes, including aerosol and cloud [see Fig. 7(a)]. A bimodal distribution separately represents aerosols and cloud. The solid curve plots a histogram of backscatters over only 2.6–2.8 km altitudes, which are definitely above the cloud threshold.

E. Multiple-Scattering Effects

Until now, we have only considered single scattering, but for low-altitude clouds, multiple scattering also affects the measurement and can lead to further discrepancies at high AOD. In general, multiple scatter is a complex process [20–22] that depends on cloud droplet size, optical depth, field of view of receiver, and laser beam spot size in clouds, etc. In fact, this paper only focuses on low-altitude optically thin clouds where the CODs are mostly smaller than 1.5, the geometric thicknesses is of the order of a few hundred meters, and the receiver field of view is 1.5 mrad. Therefore, multiple scattering may be shown to be a fairly small correction. Using a model developed by Eloranta [20], multiple-scattering factors can be first estimated with the lidar parameters and cloud profiles in Fig. 3, then the COD differences between considering only single-scattering and multiple-scattering effects are estimated in Raman retrieval [21]. Table 2 gives the percentage of multiple-scattering contributions to Raman retrievals at different droplet radii and optical depths of cloud. Clearly, multiple-scattering influences increase with the effective radius and optical depth. With the MODIS/Terra-retrieved cloud effective radius of 7.4 μm near our lidar site, we estimate that the contribution of multiple scattering is around 16–18% for low to moderate cloud optical depth. While such errors should not be ruled out, we must emphasize that these errors would apply equally to all COD methods considered. Meanwhile, with the smaller FOV (0.8 mrad), multiple-scattering influences can be largely reduced below the error estimates we have encountered.

5. Conclusion

We analyzed the retrievals of low-altitude optically thin clouds using both the N_2 Raman and elastic-scattering returns approaches. We illustrated that the elastic-return regression approach would overestimate CODs unless the aerosol correction items are accurately estimated. In particular, we showed that, by using the combined Mie–Raman returns obtained for nearby clear sky patches, we can better estimate the aerosol-scattering ratio profile, which results in a significant improvement in the COD retrieval.

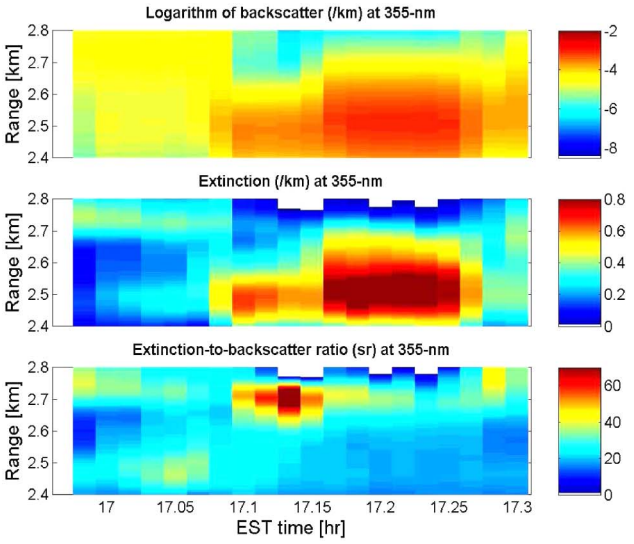

Fig. 9. (Color online) (a) Cloud backscatter, extinction, and extinction-to-backscatter ratio on 15 March 2006, (b) lidar ratio versus particle effective diameter, and (c) histogram of backscatter coefficients of aerosol and cloud on 15 March 2006.

Validation of the Raman-retrieved COD with the retrieval using the combined Raman–Mie returns has the added benefit of providing a means to assess the quality of our backscatter and extinction vertical profile in the cloud. From these measurements, we were able to provide three-dimensional profile maps of the lidar extinction/backscatter ratio (S). In particular, the S ratio statistics have a mean value near 20 sr, which was found to be consistent with a commonly used water phase cloud model. Within the water phase assumption, the lidar-ratio profiles were used for preliminary sizing of effective cloud droplet sizes, which allowed us to map areas within the cloud with small condensing droplets.

Table 2. Percentage of Multiple-Scattering Influences on Raman-Retrieved Cloud Optical Depth

	$R_e = 3.5\,\mu$m[a]	5 μm	7.4 μm[b]	10 μm
		FOV = 1.5 mrad		
COD = 0.5	6.50%	10.40%	16.20%	21.60%
COD = 1.2	7.80%	12.00%	18.00%	23.40%
		FOV = 0.8 mrad		
COD = 1.2	3.20%	5.20%	8.70%	12.30%

[a] R_e, effective radius of cloud droplet.
[b] MODIS retrieval value.

In a statistical comparison, the CODs retrieved from the Mie-returns regression method with aerosol correction and the direct Raman method show excellent agreement, and a strong correlation with $R^2 = 0.94$ and the regressed linear slope of 0.98 is observed. In general, errors between the two methods are less than 10%. However, we also show that the direct Raman method becomes less accurate at high COD since the N_2 Raman signals are attenuated by the cloud more severely than the elastic signal. This is illustrated by the fact that discrepancies between the methods grow larger when CODs are greater than 1.5. Finally, multiple-scattering effects on deriving COD were calculated for the optical parameters relevant to our study and they indicate that corrections of the order of 18% must be made. This influence can be reduced largely using the smaller field of view (FOV) of the receiver. Unfortunately, since both optical depth approaches are affected by multiple-scattering effects, no independent correction of the multiple scattering can be made.

In summary, we find that Mie-returns regression method provides the better COD measurement for the larger CODs (>1.5), although the Raman extinction method works well for COD < 1.5. However, the Mie method depends critically on the ability to estimate aerosols beneath the cloud layer, which can be best accomplished using a combined Mie–Raman lidar measurement. It is also expected that determining the cloud phase and subsequent sizing of cloud droplets within the water phase will also be significantly improved using a properly calibrated 1064 nm backscatter lidar channel; this will be discussed in a separate paper.

This work is partially supported by the research projects of National Oceanic and Atmospheric Administration (NOAA)NA17AE1625 and National Aeronautics and Space Administration (NASA) NCC-1-03009. The authors appreciate the computing codes of multiple scattering from Edwin Eloranta and Robin Hogan and the kind e-mail communications with Ulla Wandinger about multiple-scattering estimation.

References

1. C. S. Bretherton, T. Uttal, C. W. Fairall, S. Yuter, R. Weller, D. Baumgardner, K. Comstock, R. Wood, and G. Raga, "The EPIC 2001 stratocumulus study," Bull. Am. Meteorol. Soc. **85**, 967–977 (2004).
2. J. Verlinde, J. Y. Harrington, G. M. McFarquhar, V. T. Yannuzzi, A. Avramov, S. Greenberg, N. Johnson, G. Zhang, M. R. Poellot, J. H. Mather, D. D. Turner, E. W. Eloranta, B. D. Zak, A. J. Prenni, J. S. Daniel, G. L. Kok, D. C. Tobin, R. Holz, K. Sassen, D. Spangenberg, P. Minnis, T. P. Tooman, M. D. Ivey, S. J. Richardson, C. P. Bahrmann, M. Shupe, P. J. DeMott, A. J. Heymsfield, and R. Schofield, "The mixed-phase arctic cloud experiment," Bull. Am. Meteorol. Soc. **88**, 205–221 (2007).
3. D. D. Turner, A. M. Vogelmann, R. T. Austin,J. C. Barnard, K. Cady-Pereira, J. C. Chiu, S. A. Clough, C. Flynn, M. M. Khaiyer, J. Liljegren, K. Johnson, B. Lin, C. Long, A. Marshak, S. Y. Matrosov, S. A. McFarlane, M. Miller, Q. Min, P. Minnis, W. O'Hirok, Z. Wang, and W. Wiscombe, "Optically thin liquid water clouds: their importance and our challenge," Bull. Am. Meteorol. Soc. **88**, 177–190 (2007).
4. Y. J. Kaufman, I. Koren, L. A. Remer, D. Rosenfeld, and Y. Rudich, "The effect of smoke, dust, and pollution aerosol on shallow cloud development over the Atlantic Ocean," Proc. Natl. Acad. Sci. **102**, 11207–11212 (2005).
5. S. E. Schwartz, Harshvardhan, and C. M. Benkovitz, "Influence of anthropogenic aerosol on cloud optical depth and albedo shown by satellite measurements and chemical transport modeling," Proc. Natl. Acad. Sci. **99**, 1784–1789 (2002).
6. B. A. Baum and S. Platnick, "Introduction to MODIS cloud products," in *Earth Science Satellite Remote Sensing, Vol. 1: Science and Instruments*, J. J. Qu, W. Gao, M. Kafatos, R. E. Murphy, and V. Salomonson, eds. (Springer-Verlag, 2006), pp 74–91.
7. S. A. Young, "Analysis of lidar backscatter profiles in optical thin clouds," Appl. Opt. **34**, 7019–7030 (1995).
8. D. N. Whiteman, K. D. Evans, B. Demoz, D. O'C Starr, E. W. Eloranta, D. Tobin, W. Feltz, G. J. Jedlovec, S. I. Gutman, G. K. Schwemmer, M. Cadirola, S. H. Melfi, and F. Schmidlin, "Raman lidar measurements of water vapor and cirrus clouds during the passage of Hurricane Bonnie," J. Geophys. Res. **106**, 5211–5225 (2001).
9. A. Ansmann, U. Wandinger, M. Riebesell, C. Weitkamp, and W. Michaelis, "Independent measurement of extinction and backscatter profiles in cirrus clouds using a combined Raman elastic-backscatter lidar," Appl. Opt. **31**, 7113–7131 (1992).
10. B. Cadet, V. Giraud, M. Haeffelin, P. Keckhut, A. Rechou, and S. Baldy, "Improved retrievals of the optical properties of cirrus clouds by a combination of lidar methods," Appl. Opt. **44**, 1726–1734 (2005).
11. J. D. Klett, "Stable analytical inversion solution for processing lidar returns," Appl. Opt. **20**, 211–220 (1981).
12. F. G. Fernald, "Analysis of atmospheric lidar observations: some comments," Appl. Opt. **23**, 652–653 (1984).
13. A. Ansmann, M. Riebesell, and C. Weitkamp, "Measurement of atmospheric aerosol extinction profiles with a Raman lidar,"Opt. Lett. **15**, 746–748 (1990).
14. R. A. Ferrare, S. H. Melfi, D. N. Whiteman, K. D. Evans, and R. Leifer, "Raman lidar measurements of aerosol extinction and backscattering. 1. Methods and comparisons," J. Geophys. Res. **103**, 19663–19672 (1998).
15. Y. Morille, M. Haeffelin, P. Drobinski, and J. Pelon, "STRAT: an automated algorithm to retrieve the vertical structure of the atmosphere from single channel lidar data," J. Atmos. Ocean. Technol. **24**, 761–775 (2007).
16. K. J. Davis, N. Gamageb, C. R. Hagelbergc, C. Kiemled, D. H. Lenschowe, and P. P. Sullivane, "An objective method for deriving atmospheric structure from airborne lidar observations," J. Atmos. Ocean. Technol. **17**, 1455–1468 (2000).
17. E. J. O'Connor, A. J. Illingworth, and R. J. Hogan, "A technique for autocalibration of cloud lidar," J. Atmos. Ocean. Technol. **21**, 777–778 (2004).
18. R. G. Pinnick, S. G. Jennings, P. Chýlek, C. Ham, and W. T. Grandy Jr., "Backscatter and extinction in water cloud," J. Geophys. Res. **88**, 6787–6796 (1983).
19. W. L. Eberhard, "CO_2 lidar technique for observing characteristic drop size in water cloud," IEEE Trans. Geosci. Remote Sens. **31** (1), 56 (1993).
20. E. W. Eloranta, "A practical model for the calculation of multiply scattered lidar returns," Appl. Opt. **37**, 2464–2472 (1998).
21. U. Wandinger, "Multiple-scattering influence on extinction and backscatter coefficient measurements with Raman and high-spectral-resolution lidars," Appl. Opt. **37**, 417–427 (1998).
22. R. J. Hogan, "Fast approximate calculation of multiply scattered lidar returns," Appl. Opt. **45**, 5984–5992 (2006).